

Methane and carbon dioxide emissions from thermokarst lakes on mineral soils

Alex Matveev, Isabelle Laurion, and Warwick F. Vincent

Abstract: Thermokarst lakes are known to emit methane (CH₄) and carbon dioxide (CO₂), but little attention has been given to those formed from the thawing and collapse of lithalsas, ice-rich mineral soil mounds that occur in permafrost landscapes. The present study was undertaken to assess greenhouse gas stocks and fluxes in eight lithalsal lakes across a 200 km gradient of permafrost degradation in subarctic Québec. The northernmost lakes varied in their surface-water CO₂ content from below to above saturation, but the southern lakes in this gradient had much higher surface concentrations that were well above air-equilibrium. Surface-water CH₄ concentrations were at least an order of magnitude above air-equilibrium values at all sites, and the diffusive fluxes of both gases increased from north to south. Methane oxidation in the surface waters from a northern lake was only 10% of the emission rate, but at the southern end it was around 60% of the efflux to the atmosphere, indicating that methanotrophy can play a substantive role in reducing net emissions. Overall, our observations show that lithalsal lakes can begin emitting CH₄ and CO₂ soon after they form, with effluxes of both gases that persist and increase as the permafrost continues to warm and erode.

Key words: lithalsal, methane, permafrost, subarctic, thermokarst.

Résumé : Il est bien connu que les mares de thermokarst émettent du méthane (CH₄) et du dioxyde de carbone (CO₂), mais peu d'attention a été accordée jusqu'à présent à celles formées à la suite du dégel et de l'effondrement des lithalses, ces buttes minérales de sol riches en glace et présentes dans les paysages de pergélisol. La présente étude a pour objectif d'évaluer les stocks et les flux de gaz à effet de serre dans huit mares de lithalses sur un gradient de 200 km de dégradation du pergélisol dans le Québec subarctique. Les mares les plus septentrionales présentaient une teneur en CO₂ de surface inférieure ou supérieure à la saturation, alors que les lacs du sud présentaient des concentrations en surface beaucoup plus élevées, bien au-dessus de l'équilibre atmosphérique. Les concentrations de CH₄ dans les eaux de surface étaient au moins d'un ordre de grandeur au-dessus des valeurs d'équilibre à tous les sites, et les flux d'émission diffusive des deux gaz augmentaient du nord au sud. Le taux d'oxydation du CH₄ dans les eaux de surface d'une mare située au nord représentait seulement 10 % du taux d'émission, alors qu'à l'extrémité sud, il atteignait environ 60 % des émissions vers l'atmosphère. Ces résultats indiquent que la méthanotrophie peut jouer un rôle important dans la réduction des émissions nettes de CH₄. Dans l'ensemble, nos observations montrent que dans les mares de lithalses, le

Received 16 September 2017. Accepted 7 May 2018.

A. Matveev and W.F. Vincent. Centre d'études nordiques (CEN) and Département de biologie, Université Laval, Québec, QC G1V 0A6, Canada.

I. Laurion. Institut national de la recherche scientifique, Centre Eau Terre Environnement (INRS-ETE) and Centre d'études nordiques (CEN), Québec, QC G1K 9A9, Canada.

Corresponding author: Alex Matveev (e-mail: alex.matveev.1@ulaval.ca).

Warwick F. Vincent currently serves as an Associate Editor; peer review and editorial decisions regarding this manuscript were handled by Elyn Humphreys and Greg Henry.

This article is open access. This work is licensed under a Creative Commons Attribution 4.0 International License (CC BY 4.0). http://creativecommons.org/licenses/by/4.0/deed.en_GB.

CH₄ et le CO₂ pourraient être émis vers l'atmosphère peu après leur formation, à des taux qui persistent et augmentent à mesure que les lacs continuent à se réchauffer et à s'éroder.

Mots-clés : lithalse, méthane, pergélisol, subarctique, thermokarst.

Introduction

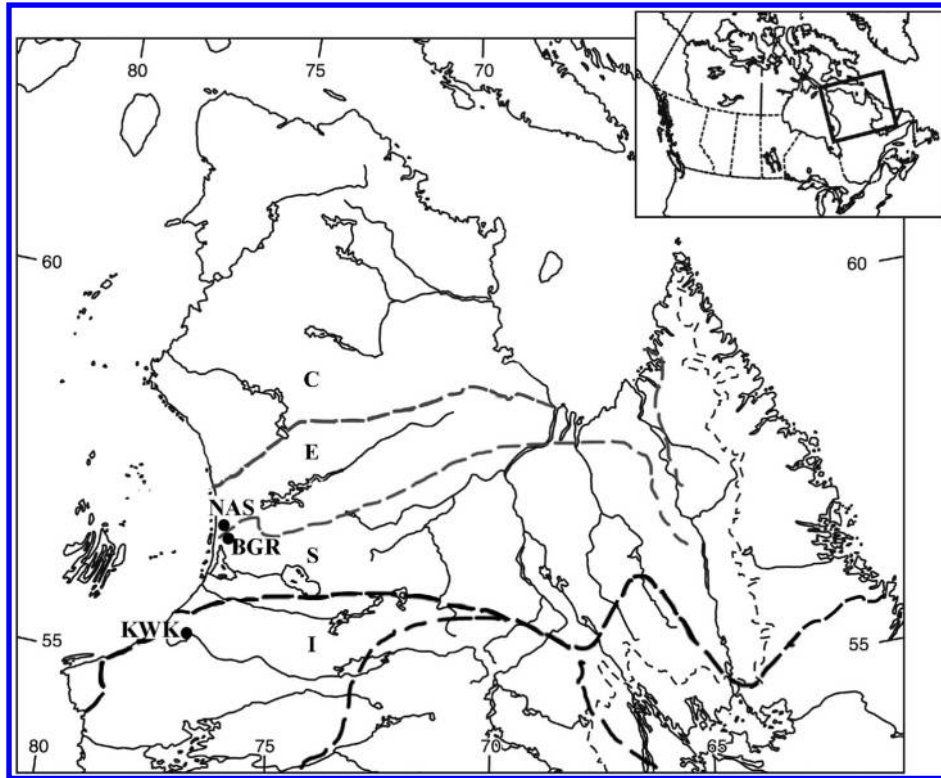
Lakes and ponds in permafrost landscapes are known to be emission sources of greenhouse gases (GHG) to the atmosphere (Tan and Zhuang 2015; Holgerson and Raymond 2016), with potentially large feedback effects on global climate (Kokelj and Jorgenson 2013; Grosse et al. 2016). Zimov et al. (1997) drew attention to the strong output of CH₄ from lakes in Siberia formed by thawing and collapse of ice-rich permafrost (thermokarst), and concluded that the CH₄ was largely derived from ancient organic carbon that had been previously stored in the frozen soils. Subsequent research suggested that this process may have accelerated the deglaciation during the early Holocene (Walter et al. 2006). A synthesis of data from boreal and Arctic lakes noted that two-thirds of the total CH₄ emissions from landscapes north of latitude 50°N is derived from freshwater systems, with thermokarst lakes contributing about 25% of that total (Wik et al. 2016). A constraint in defining the error in such estimates, however, is the poorly known extent of local and regional variability in GHG fluxes, with large variations among thermokarst lakes (Laurion et al. 2010; Sepulveda-Jauregui et al. 2015; Vonk et al. 2015).

Another major source of variability in GHG emissions from thermokarst lakes is that associated with landscape evolution (He et al. 2012; Allan et al. 2014; Lipson et al. 2015; Grosse et al. 2016). Fluxes of CH₄ to the atmosphere are thought to be especially high in newly degrading permafrost soils (Kanevskiy et al. 2014; Elvert et al. 2016), with older lakes succumbing to drainage (van Huissteden et al. 2011; Grosse et al. 2013), thereby eliminating the habitat for aquatic methanogens. Thermokarst lakes can also be subject to infilling by sediment and fen/bog vegetation, which may cause such lakes to become net sinks of carbon (Payette et al. 2004; Bouchard et al. 2017). However, the exact trajectory of geomorphological change and the associated biogeochemical effects remain uncertain in many regions of permafrost thaw and degradation.

In the subarctic region of northern Québec, Canada, two types of landscape contain permafrost mounds and associated thermokarst lakes (Allard and Seguin 1987). First, palsa landscapes occur in organic-rich peatlands, with uplifted ice-cored mounds of frozen *Sphagnum* and thermokarst lakes created by their permafrost thawing and collapse. The thermokarst lakes associated with palsas (hereafter, palsa lakes) are typically dark-coloured because of elevated concentrations of coloured dissolved organic matter (CDOM). Sunlight is strongly absorbed in their near-surface waters, and the lakes are highly stratified with anoxic conditions through most of the water column and during most of the year (Deshpande et al. 2017). These low or zero oxygen (O₂) environments are conducive to methanogenesis, and palsa lakes have strong emissions of both CH₄ and CO₂ to the atmosphere (Matveev et al. 2016). Another type of terrain occurs on mineral soils as lithalsa landscapes (Calmels et al. 2008), with frost-heaved, clayey, silt-rich permafrost mounds, and associated thermokarst lakes (hereafter, lithalsa lakes). Lithalsa lakes are more varied in colour, from blue-green to white to brown (Watanabe et al. 2011), and are also known for their stratified structure and anoxic bottom waters (Deshpande et al. 2015). Like palsa lakes, they accumulate CH₄ and CO₂ (Laurion et al. 2010) and have high rates of bacterial heterotrophic production (Breton et al. 2009; Roiha et al. 2015).

The aim of the present study was to provide an improved understanding of GHG stocks (specifically CO₂ and CH₄) in lithalsa lakes, and of the emission fluxes from such lakes at

Fig. 1. Study region and permafrost distribution in Nunavik (QC, Canada). The studied sites NAS, BGR, and KWK are indicated as black dots on the eastern shore of the Hudson Bay. Permafrost types in the region of study (Allard and Seguin 1987) are shown with each type separated by dashed lines, where C, E, S, and I indicate the zones of continuous permafrost (C, 90%–100% of land area underlain by permafrost), discontinuous extended (E, 50%–90%), discontinuous sporadic (S, 10%–50%), and isolated patches of permafrost (I, 0%–10%).



different stages of permafrost degradation. We hypothesized that stocks and emissions increase with increasing degree of permafrost degradation, with greatest effects at the warm southern margin of Arctic permafrost landscapes. This hypothesis implies that the northward contraction of permafrost will be accompanied by increased rates of emission, which could continue well after lake formation. We evaluated this hypothesis by making measurements at a series of lithalsa lakes across a gradient of permafrost conditions in sub-arctic Québec, including at the southern limit of current permafrost extent where thermokarst lakes have formed and persisted for at least many decades.

Materials and methods

Study sites

Sampling was in the western Hudson Bay area of Nunavik (Northern Quebec, Canada; Fig. 1), a region experiencing rapid warming and landscape change (Bhiry et al. 2011), and the location of multiple research sites within the program “Arctic Development and Adaptation to Permafrost in Transition” (ADAPT; Vincent et al. 2017) that this study was part of. The region spans four different permafrost zones, from continuous and discontinuous widespread permafrost in the north, to sporadic and isolated permafrost in the south (Allard and Seguin 1987; Vallée and Payette 2007), with mean annual air temperatures over that geographical range from -4.7 to -2.8 °C. Sampling of lithalsa lakes was at three sites

across this north–south gradient (Fig. 1), namely: (a) in discontinuous widespread permafrost, north of the Nastapoka River (56.9°N, 76.3°W; NAS lakes); (b) in discontinuous permafrost, 20 km east of the village of Umiujaq (56.6°N, 76.2°W; BGR lakes); and (c) in degraded sporadic permafrost, 13 km north of the village of Whapmagoostui-Kuujuarapik and around 200 km south of the NAS site (55.2°N, 77.5°W; KWK lakes; Supplementary Fig. S1 and associated video¹; additional descriptions are given in Bégin and Vincent 2017).

Lake sampling and physical, chemical, and biological properties

In situ measurements and samples were collected from eight lakes at the three sites (Fig. 1 and Supplementary Table S1¹) during the summer open-water period, from 2012 to 2015. Vertical profiles of physicochemical properties were obtained from an inflatable boat transported to the sites by helicopter, with a YSI 6000 multi-probe (Yellow Springs Instruments, Yellow Springs, OH, USA) and an RBR Concerto conductivity–temperature–depth logger (RBR Ltd., Ottawa, ON, Canada). The accuracy of these measurements was ± 0.15 °C, ± 0.2 pH units, ± 0.2 mg oxygen L⁻¹, and ± 0.001 mS cm⁻¹ conductivity for the YSI; and ± 0.002 °C and ± 0.003 mS cm⁻¹ for the RBR. Underwater photosynthetically active radiation (PAR) irradiance was measured with a Licor submersible radiometer.

Samples for water analysis were collected at the surface and bottom of the water column, filtered at the Centre for Northern Studies (CEN) research station in Whapmagoostui-Kuujuarapik, and then shipped to home facilities (Laval University and INRS, Québec City, QC, Canada) for laboratory analysis. Samples for analysis of soluble reactive phosphorus (SRP) were filtered through 0.2 µm cellulose acetate filters and then analyzed using a colorimetric method (Standard Methods 4500-P.E., APHA, AWWA, and WEF 1998) and a Lachat Autoanalyzer (Lachat QuikChem® 8500 Series 2 Flow Injection Analysis System, Hach Company, Loveland, CO, USA). For total phosphorus (TP), unfiltered samples were acidified with 15% H₂SO₄, digested with persulfate and analyzed for SRP as above. For dissolved organic carbon (DOC) concentrations, filtered (as above) lake water samples were acidified to remove inorganic carbon, and analyzed by high temperature catalytic combustion method with infrared detection (Standard Methods 5310 B, APHA, AWWA, and WEF 1998) in a Shimadzu VCPH analyzer (Shimadzu Scientific Instruments, Columbia, MD, USA). The total nitrogen content (TN) was measured from unfiltered water samples by alkaline digestion with persulfate, followed by analysis by the sulfanilamide colorimetric method after reduction with cadmium in a Lachat Autoanalyzer (QuikChem® Method 10-107-04-3-A). Total suspended solids (TSS) were determined by weight after filtration onto precombusted, preweighed glass fiber filters (nominal porosity of 0.7 µm). Chlorophyll *a* concentration (Chl-*a*) was measured by high-pressure liquid chromatography from pigments extracted with 95% MeOH from the above glass fiber filters kept frozen at -80 °C until analysis, as in Bonilla et al. (2005).

Automated lake surface observations

Automated cameras (Reconyx PC800, Holmen, WI, USA) were installed on the shores of three thermokarst lakes (one per study site, respectively, KWK12, BGR1, and NASa) at a distance of 5–10 m from the edge of the summer water extent. The cameras recorded six photographs per 24 h period at 1 h intervals between 1000 and 1500 (Eastern Standard Time, EST). The data were retrieved annually at the end of August each year. The complete dataset is archived in the Nordicana D data repository (Pienitz et al. 2017). These data were used to calculate the number of days of open water for each site, including for the gas flux calculations.

¹Supplementary material is available with the article through the journal Web site at <http://nrcresearchpress.com/doi/suppl/10.1139/as-2017-0047>.

CH₄ and CO₂ measurements

Profiles of CH₄ and CO₂ concentrations were obtained from discrete depth samples, as in [Deshpande et al. \(2017\)](#), and with continuous automated dissolved gas monitoring systems. The discrete depth samples were obtained in triplicate with a thin-layer laminar-flow sampler that had two plates set 63.5 mm apart ([Matveev et al. 2016](#)), at 0.1–0.5 m depth intervals. The samples were transferred with a peristaltic pump to a 2 L prerinsed, low density polyethylene bottle. The lake water was then equilibrated with a 20 mL air-filled headspace, and a 10 mL gas sample taken and injected into a 5.9 mL helium-flushed, evacuated borosilicate glass vial (Labco Exetainer[®], Labco Limited, Lampeter, UK). The gas samples were subsequently analyzed for CH₄ and CO₂ by gas chromatography with flame ionization detection (Varian 3800, COMBI PAL head space injection system, CP-Poraplot Q 25 m with flame ionization detector) as in [Matveev et al. \(2016\)](#).

The surface fluxes of CH₄ and CO₂ were calculated from the dissolved gas concentrations at the air–water interface as in [Matveev et al. \(2016\)](#). We used a wind-based model, with correction for turbulence and low-solubility gases as in [Vachon et al. \(2010\)](#). The gas flux F_i for each gas i was expressed assuming molecular diffusion as

$$(1) F_i = k_i K_{Hi} \Delta P_i$$

where K_{Hi} is the Henry Law constant, k_i is the gas transfer velocity, and ΔP_i is the gradient of the gas partial pressures at the air–water interface.

Two automated systems were used, depending on sampling conditions: (1) a “CO₂-box” continuous GHG monitoring system that simultaneously measured dissolved CO₂, CH₄, and O₂ contents in a gas stream continuously equilibrated with the source water ([Carignan 1998](#), details in [Laurion et al. 2010](#)) and (2) a Franatech METS system composed of an infrared-CO₂ sensor and a semi-conductor CH₄ sensor (Franatech GmbH, Lüneburg, Germany) in separate housings and assembled on a flow-through chamber with a constant water flow produced with a submersible pump (model SBE-5T, Sea-Bird Electronics, Inc., Bellevue, WA, USA). The two instruments were cross-calibrated and the datasets combined (an example of the consistency among methods is given in Supplementary Fig. S2¹).

Gas concentrations in the littoral zone were measured with the CO₂-box deployed from the shore (KWK12 and BGR1), whereas concentrations in the deepest offshore water and for the NASA transect were measured with the Franatech METS instrument deployed from the boat. The intake of the CO₂-box was submerged to 5–10 cm from the surface, with the peristaltic pump located inside the instrument housing; the METS intake was a 15 cm tube connected to a submersible Seabird pump, and the entire instrument was submerged at around 10 cm depth from the surface for surface samples.

Ebullition of CH₄ and CO₂ was assessed at KWK and BGR sites by collecting gas samples with submerged, opaque, inverted cones, with a 0.5 m² opening at the bottom and a syringe equipped with a valve at the top (details in [Matveev et al. 2016](#)). Two to three gas traps per lake were installed for 1–30 days, depending on ebullition rates and logistic constraints. The gas samples were stored in 12 mL or 5.9 mL Labco Exetainer[®] vials, prepared as above. Sampling dates and numbers of ebullition samples for each lake are given in Supplementary Table S2,¹ which also provides the sampling dates for dissolved gas concentrations measured by the headspace, CO₂-box, and METS profiler methods, as described above.

The CH₄ oxidation rates were calculated as a linear regression from concentrations measured every 3 h by subsampling a closed vessel containing 20 L of surface lake water connected to the CO₂-box. The incubations were performed in the laboratory under ambient temperature (ca. 15 °C) and low light (<50 μmol photons m⁻² s⁻¹).

Isotopic composition and radiocarbon

Samples for CO₂ and CH₄ radiocarbon dating (¹⁴C isotope) were collected in helium-flushed, evacuated 50 mL serum bottles (Wheaton, IL, USA) from two gas ebullition samples collected from funnels installed in lake BGR1 in 2014. The ¹⁴C content of CO₂ and CH₄ was measured by accelerator mass spectrometry in the Keck Carbon Cycle AMS Facility of the University of California Irvine (Irvine, CA, USA), as in [Matveev et al. \(2016\)](#). The ¹⁴C ages were expressed as fractions of the modern standard (Δ¹⁴C) following [Stuiver and Polach \(1977\)](#), with all results corrected for isotopic fractionation.

The δ¹³C isotopic fractionation was assessed in the ebullition and the discrete depth samples, all collected in triplicates by the headspace method and stored in 12 mL Exetainer® vials, prepared as above. The δ¹³C in CH₄ and CO₂ was measured at the GRIL-UQAM facility (Montreal, QC, Canada) by continuous-flow cavity ring-down spectroscopy (CRDS) with near-infrared laser source method, using a Picarro (Picarro Inc., Santa Clara, CA, USA) “G2201-i δ¹³C in CH₄ and CO₂ Gas Analyzer” (<0.12‰ δ¹³C-CO₂ and <0.4‰ δ¹³C-CH₄ precision at 1-σ, 1 h window, 5 min average). The results were expressed as the δ¹³C ratio of a sample relative to the Vienna Pee Dee Belemnite (VPDB) international measurement standard ([Coplen 2011](#)). The isotope separation factor between δ¹³C-CO₂ and δ¹³C-CH₄ (ϵ_C) was calculated according to [Whiticar \(1999\)](#).

$$(2) \quad \epsilon_C = \delta^{13}\text{C-CO}_2 - \delta^{13}\text{C-CH}_4$$

The δ¹³C-CO₂ – δ¹³C-CH₄ carbon isotope partitioning resulting from microbial CH₄ production and oxidation was further expressed as a combination plot of the δ¹³C-CO₂ versus δ¹³C-CH₄, as in Fig. 8 of [Whiticar \(1999\)](#).

Results

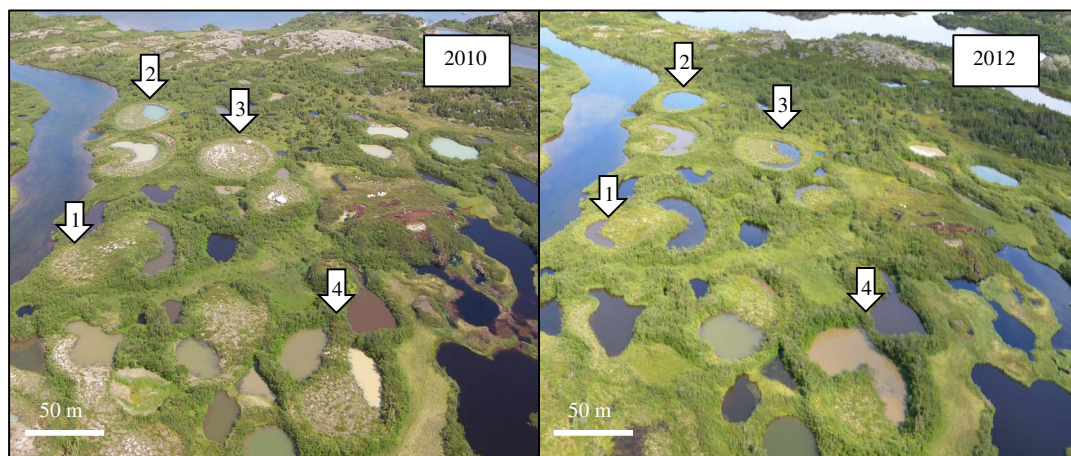
Morphometry

The lithalsa lakes were all shallow, with an average (±SD) depth of 2.7 (±1.1) m (Supplementary Table S1¹), and a distinct morphometry with steep, eroded shores (Supplementary Fig. S2¹). The maximum depths were relatively stable among sampling years at KWK and NAS from 2012 to 2015, but BGR1 increased by 0.6 m to a maximum of 4.4 m, while BGR2 increased by 0.25 m to a maximum of 1.55 m. The mean surface area of the studied lakes averaged 942 m² with large variations among sites [coefficient of variation (CV) = 94%], but much less between lakes within each site (average CV = 19%). Within this limited data set, the average lake area per site decreased as a function of distance ($R^2 = 0.88$ for the linear regression) southwards in the study region (Supplementary Fig. S3 and Table S1¹). There were no observed changes during the period of observation in lake area at KWK and NAS sites, but the BGR site showed further evidence of rapid landscape change. Some of the lithalsa mounds experienced thawing and collapse (thermokarst), producing new lithalsa lakes (e.g., BGRb), and there were also increases in area of some lakes (e.g., BGR1 and BGR2) and fusing of adjacent water bodies (Fig. 2).

Ice regime and winter snow accumulation

The automated camera records showed the lakes were ice-covered for around eight months each year. At the lake NASa (site NAS), the lake ice formed at the beginning of November (2014), with an overlying layer of snow that accumulated to a maximum thickness of 0.8 m (winter 2015). The ice first broke up during the last week of April (2015), but quickly reformed, with final break-up and disappearance during the first 2 weeks of June (2015). At the BGR site, the lake ice broke up on lake BGR1 during the last week of May

Fig. 2. Morphological changes at the BGR site from 2010 to 2012, seen at oblique aerial photographs made with a two-year interval, showing permafrost degradation (thermokarst process). New thermokarst lakes were formed (1, 3). The existing lithalsa lakes, including the studied lakes BGR1 and BGR2 (2), increased in surface area or merged with adjacent water bodies (4). The reference scale on the images is approximate.



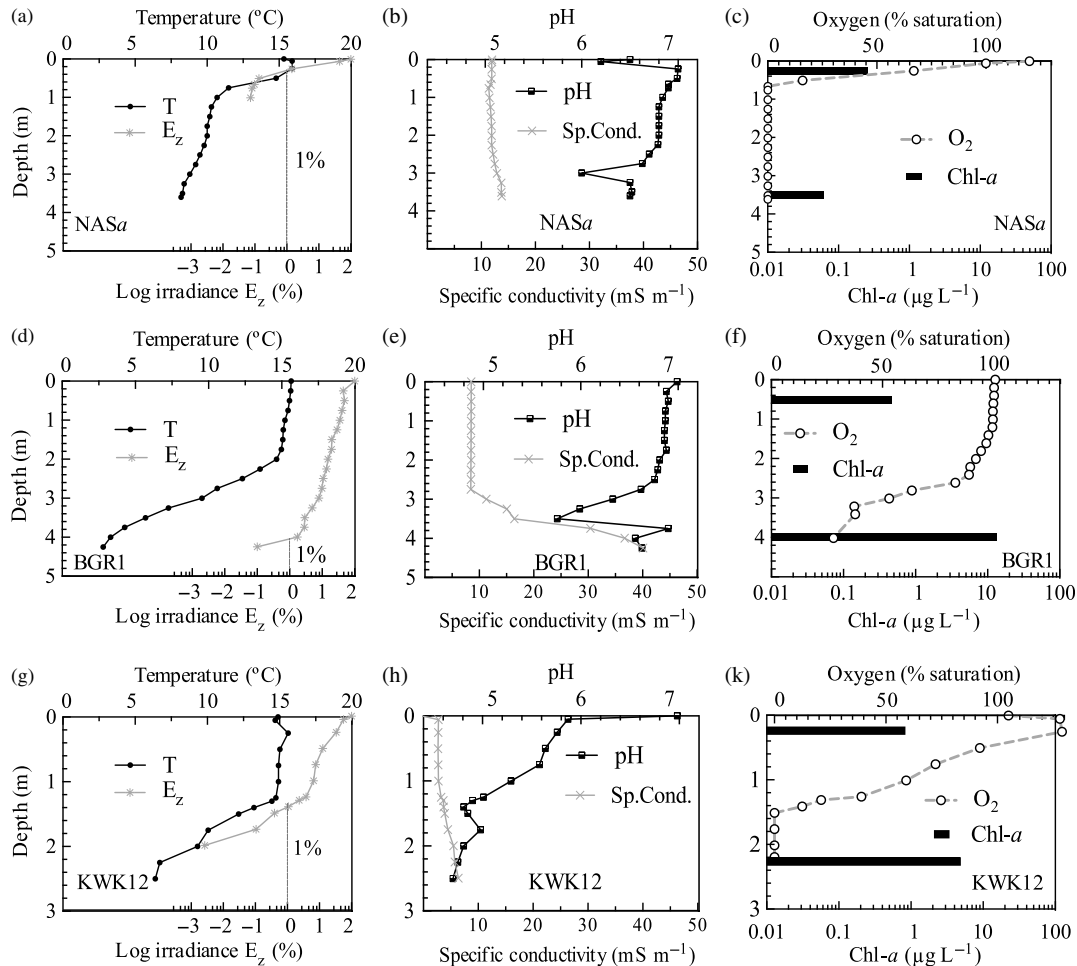
(2015), and the open-water period extended from the first week of June to the second week of October (2016). The maximum winter snow accumulation was around 0.7 m (winter 2016). The ice-free period recorded at the lake KWK12 (in the southern KWK valley) was about 2 weeks longer than in BGR (from the last week of May to the third week of October 2016), with a maximum winter (2016) snow accumulation of ca. 0.6 m. None of the three lake ice records showed any evidence of persistent gas bubbling (“bubbling hot-spots” as in Wik et al. 2011) on images with clear ice during its formation and break-up.

Limnological properties

All of the lithalsa lakes were thermally stratified during the period of observation, with the shallowest thermocline occurring at 0.5 m depth in NASA (Fig. 3a), possibly linked to the strong light attenuation in its turbid waters (surface TSS = 319 mg L⁻¹, Table 1). The surface mixing zone was 2 and 1.5 m deep in the lakes BGR1 and KWK12, respectively (Figs. 3d, 3g). The depth of the euphotic zone (1% of surface PAR) similarly varied among the lakes, from 0.55 m in NASA to 4.1 m (to the lake bottom) in BGR1 (Figs. 3a, 3d, 3g). The pH was close to neutral in most lakes of NAS and BGR sites (Figs. 3b, 3e), while it was significantly lower in KWK lakes ($p < 0.0001$ in two-way ANOVA per site comparison), falling to acidic values of 4.6 at the bottom of KWK12 (Fig. 3h). Specific conductivity values varied from 2.7 to <15 mS m⁻¹ in most lakes of different permafrost regions, typically increasing with depth by about 50% (Figs. 3b, 3h), with the exception of BGR1, where it sharply increased up to 40.1 mS m⁻¹ below the mixing zone (Figs. 3d, 3e).

TN and TP concentrations were variable among lakes in all sites (Table 1), with no significant difference between the top and bottom of the water column ($p > 0.1$, Wilcoxon’s test). SRP averaged high values (3.5 µg P L⁻¹) but was similarly variable in all lakes (CV = 85%), and with no significant difference between the top and bottom of the water column ($p = 0.12$, Wilcoxon’s test). The lakes had substantial concentrations of TSS in their bottom waters, with exceptionally high values throughout the water column of NASA (Table 1). DOC concentrations (all depths combined) were significantly higher ($p = 0.007$, *t* test) in

Fig. 3. Vertical profiles of the measured physical, chemical, and biological characteristics in one representative lake from each of the three study sites located in the discontinuous widespread (NASa; top panels), discontinuous (BGR1; middle panels), and sporadic (KWK12; bottom panels) permafrost (data from August 2014 shown).



the southern KWK lakes versus northern lakes (BGR and NAS, Table 1), averaging 14.5 and 4.9 mg C L^{-1} , respectively. Chl- a concentrations (all depths combined) were also significantly higher ($p = 0.025$, t test) in the southern (mean of 16.9 $\mu\text{g L}^{-1}$) versus northern (mean of 2.5 $\mu\text{g L}^{-1}$) lakes.

Dissolved gas concentrations

Dissolved O_2 concentrations were typically at saturation at the surface of all lakes, with undersaturation at depth, whereas CH_4 and CO_2 concentrations varied considerably among sites, lakes, and lake depths (Fig. 4). CO_2 concentrations increased toward the bottom in all lakes. CH_4 concentrations also increased with depth in KWK and BGR lakes (Figs. 4c–4f), but were similar throughout the water column in NAS lakes (Figs. 4a, 4b).

Unlike other lakes, the surface waters of lake NASa were undersaturated in CO_2 to the depth of 1 m (Fig. 4a) and this gas was in low concentration to 3 m in NASh (Fig. 4b). In lakes of the BGR site, surface CO_2 values varied from 29.9 $\mu\text{mol L}^{-1}$ in BGR1 and 20.5 $\mu\text{mol L}^{-1}$ in

Table 1. Biogeochemical properties of the studied lakes, including total nitrogen (TN), total phosphorus (TP), soluble reactive phosphorus (SRP), chlorophyll *a* (Chl-*a*), total suspended solids (TSS), dissolved organic carbon (DOC), and dissolved CO₂ and CH₄ concentrations.

Lake	TN (mg N L ⁻¹)	TP (mg P L ⁻¹)	SRP (µg P L ⁻¹)	Chl- <i>a</i> (µg L ⁻¹)	TSS (mg L ⁻¹)	DOC (mg C L ⁻¹)	CO ₂ (µmol L ⁻¹)	CH ₄ (µmol L ⁻¹)
Surface								
KWK1	1.08	0.47	5.0	8.7	14	17	32	0.1
KWK11	1.01	0.12	<3	24	8.3	27	42	0.13
KWK12	0.41	0.02	0.4	5.6	2.4	6.3	44	0.9
BGR1	0.24	0.01	0.4	1.0	2.0	2.4	30	0.8
BGR2	0.43	0.04	3.3	0.9	5.9	10	20	0.5
BGRb	0.11	0.01	4.1	—	10	4.1	43	0.4
NASa	4.22	0.13	2.9	3.0	319	3.0	15	0.13
NASh	0.60	0.03	6.2	3.6	18	4.1	30	0.19
Bottom								
KWK1	0.94	0.05	11	19	188	12	807	190
KWK11	0.57	0.02	<3	39	27	18	731	40
KWK12	0.63	0.07	1.8	5	6	8	762	710
BGR1	0.51	0.06	2.1	4.6	14	3	382	197
BGR2	—	—	—	—	31	10	193	3
NASa	4.14	0.18	19	2	810	2	97	0.02

BGR2, to 42.5 µmol L⁻¹ in the newly formed lake BGRb (Table 2). All these were above the air-equilibrium value of about 16.7 µmol L⁻¹ (Fig. 5). Surface CO₂ concentrations were less variable and generally higher in KWK lakes relative to those in the north, averaging 45.4 ± 13.2 µmol L⁻¹. The CH₄ concentration at the surface of NAS lakes varied from 0.027 to 0.21 µmol L⁻¹ (Table 2), all at least an order of magnitude above the air-equilibrium value of about 0.0031 µmol L⁻¹ (Fig. 5). The CH₄ concentrations in BGR lakes were much higher, from 0.35 to 0.80 µmol L⁻¹ (Figs. 4c, 4d), and averaged 0.41 µmol L⁻¹ (Table 2). KWK lakes also had high surface CH₄ concentrations averaging 0.43 µmol L⁻¹, including the highest encountered in this study, and large variability among lakes (CV = 78%).

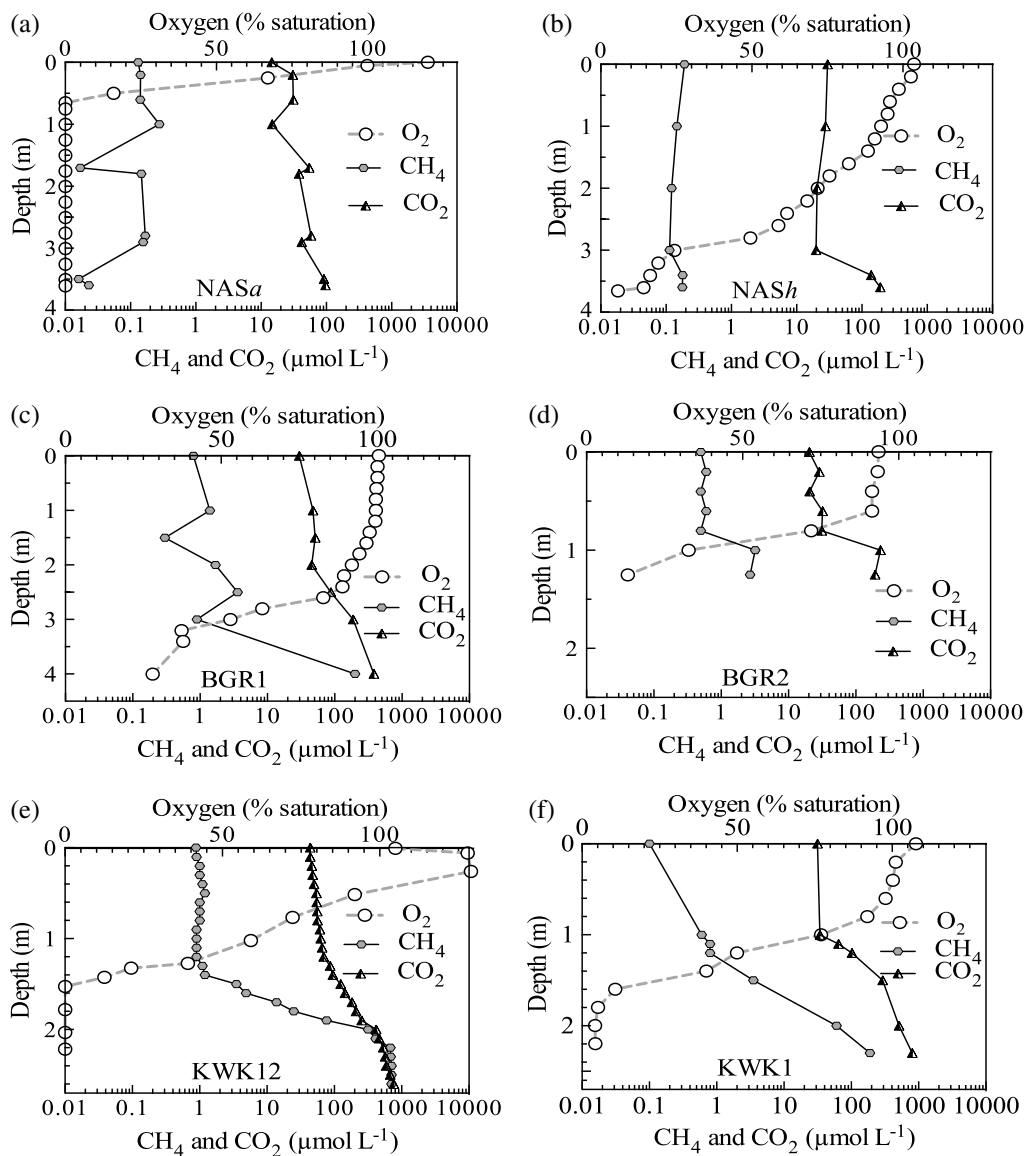
The bottom waters of all lakes were supersaturated in CH₄ and CO₂, with concentrations 2–3 orders of magnitude higher than at the surface (Figs. 4, 5). The vertical gradients were much steeper in KWK lakes compared with those in NAS lakes and in some of the BGR lakes (Fig. 4); BGR1 (Fig. 4c) and the newly formed BGRb (Supplementary Fig. S4¹) also had steep gradients in CO₂ and CH₄ concentrations towards the bottom. The bottom concentrations of CH₄ and CO₂ were one or more orders of magnitude higher in the lakes of the southern KWK site (mean ± SD: 1259 ± 1066 µmol CO₂ L⁻¹ and 310 ± 281 µmol CH₄ L⁻¹) relative to those of the northernmost NAS site (120 ± 58 µmol CO₂ L⁻¹ and 0.14 ± 0.08 µmol CH₄ L⁻¹). Values at the BGR sites (1081 ± 1402 CO₂ L⁻¹ and 162 ± 165 µmol CH₄ L⁻¹) were similar to or below those at KWK; however, the lake-to-lake variability at all sites was considerable, as shown by the large SD values.

To examine lateral variations in GHG concentrations, we sampled one of the larger lakes (NASa) in duplicate at the surface and below the surface (0.7–1.0 m depth) at five stations extending from one side of the lake to the other (Fig. 6). The variation in CH₄ concentrations was small, with CVs of 8% (surface) and 9% (subsurface). The CO₂ variation was slightly larger, with CVs of 23% (surface) and 20% (subsurface), with the lowest concentrations measured in the littoral zone at each end of the transect.

CH₄ and CO₂ fluxes

The diffusive CO₂ flux from Nunavik lithalsa lakes gradually increased towards the south in the region of study (Table 3). The values ranged from a net sink of -1.7 mmol CO₂ m⁻² day⁻¹ (in lake NASa) to a source of up to 30.8 mmol CO₂ m⁻² day⁻¹ in lake KWK12

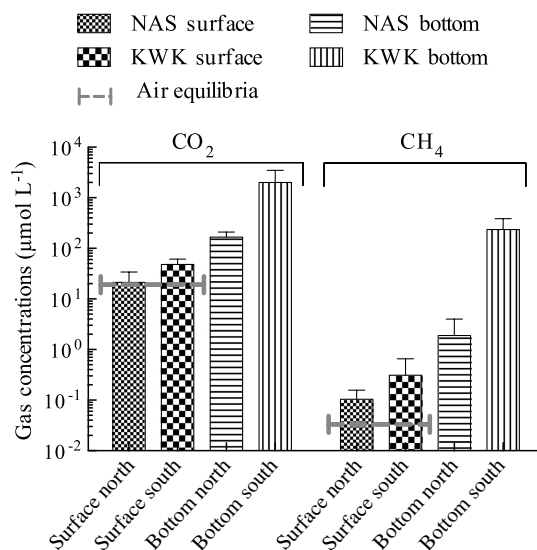
Fig. 4. Gas concentration profiles in representative lakes from each of the three study sites located in the discontinuous widespread (NAS profiles from 7 August 2012), discontinuous (BGR profiles from 9 August 2012), and sporadic (KWK profiles from 25 August 2015) permafrost.



(Table 4), with an intermediate value of $8.1 \pm 7.7 \text{ mmol CO}_2 \text{ m}^{-2} \text{ day}^{-1}$ on average in BGR lakes. Although the CO_2 flux at NAS was on average negative, it alternated between positive and negative values both within one lake and between the lakes of this site at different visits ($\text{CV} = 168\%$). The average diffusive flux of CO_2 from the southern KWK lakes ($20.2 \pm 7.1 \text{ mmol CO}_2 \text{ m}^{-2} \text{ day}^{-1}$) was more than double that from BGR, and an order of magnitude greater than from NAS lakes. There was no significant correlation between the concentrations of DOC and CO_2 in these lakes (Table 1; $r = 0.33$, $p = 0.42$ for surface waters; $r = 0.63$, $p = 0.2$ for bottom waters). The diffusive CO_2 fluxes were several orders of magnitude greater than the CO_2 ebullition fluxes, the latter only measured in BGR and KWK lakes

Table 2. Average (summer 2012–2015) surface CH₄ and CO₂ concentrations per study site.

Gas concentration	Study site		
	NAS	BGR	KWK
CO₂ surface			
Mean (μmol L ⁻¹)	23.6	33.0	45.5
Coefficient of variation (%)	40	25	25
Number of measurements (<i>n</i>)	12	11	8
CH₄ surface			
Mean (μmol L ⁻¹)	0.15	0.41	0.43
Coefficient of variation (%)	44	54	78
Number of measurements (<i>n</i>)	12	11	8

Fig. 5. Surface and bottom CH₄ and CO₂ concentrations at the northernmost (NAS) and southernmost (KWK) sites (average for summer observations from 2012 to 2015).

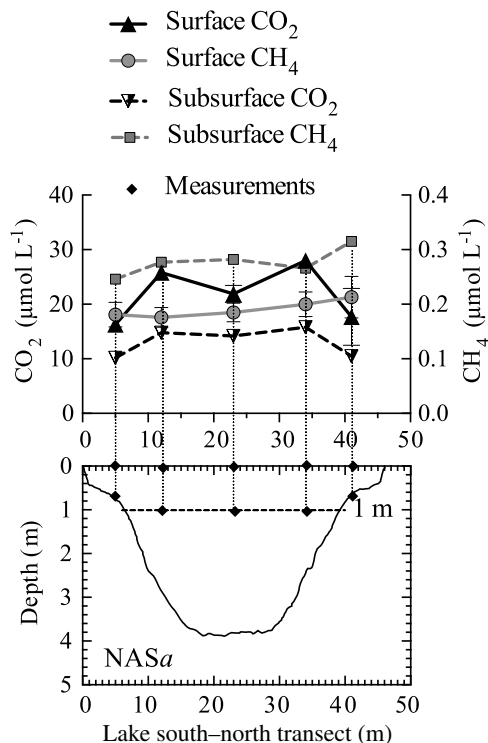
(Table 3). However, the CO₂ ebullition flux was an order of magnitude greater at the BGR site (0.01 mmol CO₂ m⁻² day⁻¹) relative to KWK (0.006 mmol CO₂ m⁻² day⁻¹).

The positive southward gradient was also observed in the CH₄ diffusion rates from these Nunavik lithals lakes (Table 3). The diffusive CH₄ fluxes at the NAS site were always positive (0.12 ± 0.03 mmol m⁻² day⁻¹), and with low variability between the lakes (CV = 25%). Diffusive emissions from BGR lakes averaged 0.45 ± 0.06 mmol CH₄ m⁻² day⁻¹, in the same order of magnitude than from KWK lakes that showed greater variability (0.47 ± 0.33 mmol CH₄ m⁻² day⁻¹). Similar to the observations for CO₂, the mean CH₄ ebullition from the BGR site on discontinuous permafrost (0.26 mmol CH₄ m⁻² day⁻¹) was an order of magnitude greater than that from the KWK site in the largely degraded isolated permafrost region (0.016 mmol CH₄ m⁻² day⁻¹). Overall, the observed total CH₄ fluxes from the studied lakes were within the range of values observed in other thermokarst lakes in the circumpolar region, and the CO₂ fluxes were at the upper limit or above the values reported elsewhere (Table 4).

Isotopic fractionation and ¹⁴C-dating of GHG

In general, the δ¹³C isotopic signatures in dissolved gases were similar in surface waters of the lithals lakes (Table 5), with the exception of a low δ¹³C-CH₄ value in the surface water

Fig. 6. Dissolved gas concentrations measured along the south–north transect crossing lake NASa on 24 August 2014 at the surface and at 1 m depth. The bottom panel shows the bathymetry (from Proult 2014) and corresponding stations on the lake.



of newly formed lake BGRb. The bottom water $\delta^{13}\text{C}$ signatures differed significantly from those at the surface in KWK lakes for $\delta^{13}\text{C}\text{-CH}_4$ (paired $t = 5.8$, $p = 0.01$) but not for $\delta^{13}\text{C}\text{-CO}_2$ (paired $t = 2.3$, $p = 0.07$), and for neither gas in the BGR lakes ($\delta^{13}\text{C}\text{-CH}_4$: paired $t = 1.5$, $p = 0.15$; $\delta^{13}\text{C}\text{-CO}_2$: paired $t = 0.6$, $p = 0.3$). There was greater $\delta^{13}\text{C}$ depletion in CH_4 relative to CO_2 in all samples, as expected (Table 5). For all lakes, the isotope separation factor between $\delta^{13}\text{C}\text{-CO}_2$ and $\delta^{13}\text{C}\text{-CH}_4$ (ϵ_C) averaged ($\pm\text{SD}$) $-29.1\% \pm 7.1\%$ in the surface waters, and $-40.4\% \pm 6.5\%$ in the bottom waters (Fig. 7), and there was also a significant difference in ϵ_C between the surface and bottom waters of KWK lakes (paired $t = 5.5$, $p = 0.03$) but not BGR lakes (paired $t = 1.1$, $p = 0.40$). The $\delta^{13}\text{C}\text{-CH}_4$ measured in the single BGR1 ebullition sample was -65.6% , which was more depleted than the lowest dissolved CH_4 value for this lake ($\delta^{13}\text{C}\text{-CH}_4$ of -55.2% in the bottom waters).

The ^{14}C -age of the ebullition gases collected from lake BGR1 was also highly variable, with the oldest carbon contained in the CO_2 . The $\Delta^{14}\text{C}$ values measured in the CO_2 in this lake ranged from $-225\% \pm 10.6\%$ to $-517.1\% \pm 4.7\%$, corresponding to the age range from 1990 ± 110 to 5790 ± 80 years before present (years B.P.), respectively. The $\Delta^{14}\text{C}$ values measured in CH_4 in this lake ranged from $34.4\% \pm 17.3\%$ to $83.7\% \pm 1.8\%$, corresponding to modern age (100–320 years B.P.).

CH_4 oxidation rates

Concentrations of CH_4 during the two laboratory incubations of lake water decreased linearly with time over the 27–48 h duration of the experiments, while CO_2 concentrations increased (Fig. 8). These net CH_4 consumption rates were an order of magnitude higher for

Table 3. Average (summer 2012–2015) CO₂ and CH₄ flux (diffusion and ebullition) and their greenhouse gas forcing per study site (given as CO₂-equivalent*).

Gas flux	Study site		
	NAS	BGR	KWK
CO₂ ebullition			
Mean rate (mmol m ⁻² day ⁻¹)	—	0.01	0.006
Mean rate (mg CO ₂ m ⁻² day ⁻¹)	—	0.4	0.26
Coefficient of variation (%)	—	132	116
Number of measurements (n)	—	2	2
CO₂ diffusion			
Mean rate (mmol m ⁻² day ⁻¹)	3.4	8.1	20.2
Mean rate (mg CO ₂ m ⁻² day ⁻¹)	150	357	889
Coefficient of variation (%)	169	95	35
Number of measurements (n)	6	6	6
CH₄ ebullition			
Mean rate (mmol m ⁻² day ⁻¹)	—	0.26	0.016
Mean rate (mg CO ₂ -eq m ⁻² day ⁻¹)*	—	117	7
Coefficient of variation (%)	—	136	132
Number of measurements (n)	—	2	2
CH₄ diffusion			
Mean rate (mmol m ⁻² day ⁻¹)	0.12	0.45	0.47
Mean rate (mg CO ₂ -eq m ⁻² day ⁻¹)	54	202	211
Coefficient of variation (%)	25	12	70
Number of measurements (n)	6	6	6
Total greenhouse gas forcing			
Per study region (mg CO ₂ -eq m ⁻² day ⁻¹)	204 [†]	676	1108
Average lake area (m ²)	2035	728	427
Open water period (days)	133	134	145
Per lake per open water period (kg CO ₂ -eq year ⁻¹)	55 [†]	66	68

Note: Yearly estimates are for the open water period, as determined from the automated camera images.

*For methane, CO₂-equivalent (CO₂-eq.) = CH₄ (mg CH₄ m⁻² day⁻¹) × 28, to consider its global warming potential over 100 years, as in Myhre et al. (2013).

[†]Diffusion only.

Table 4. The diffusive and ebullition flux of CH₄ and CO₂ from lithalsa lakes (2012–2015 average) compared with other lakes in the circumpolar region.

	Canada				Finland	Alaska	Siberia
	Lithalsa (mineral) [1]	Palsa (peatland) [2]	Tundra lakes [3]	High Arctic [4]	Permafrost boreal [5]	Continuous yedoma [6]	Tundra (peatland) [7]
Site [Ref.*]							
Latitude (°N)	55–57	55–57	73	82	61.5	60–68	65
CH₄ ebullition							
Mean rate (mmol m ⁻² day ⁻¹)	0.1	0.2	16.9	0.001	0.9	5.5	0.2
Range	0.02–0.25	<0.01–0.8	0.00–535	0.00–0.01	0.2–1.5	2.2–7.2	0.04–0.3
CH₄ diffusion							
Mean rate (mmol m ⁻² day ⁻¹)	0.4	3.3	0.8	0.7	0.7	0.9	0.4
Range	0.07–0.82	0.01–12.8	0.03–5.8	0.00–1.34	0.1–2.0	0.6–1.1	0.2–0.6
CO₂ ebullition							
Mean rate (mmol m ⁻² day ⁻¹)	0.1	0.01	0.7	0.002	0.3	0.11	0.005
Range	0.006–0.2	0.001–0.1	0.00–16.3	0.00–0.01	0.002–0.5	0.01–0.14	0–0.03
CO₂ diffusion							
Mean rate (mmol m ⁻² day ⁻¹)	12.3	58.3	8.7	7.2	17.0	133.9	34.1
Range	–1.7 to 30.8	4–242	–12 to 65	0.00–165	9–25	4.6–263	11.4–59

*References in the table: [1] This study, [2] Matveev et al. 2016, [3] Bouchard et al. 2015, [4] Emmerton et al. 2016, [5] Huttunen et al. 2003, [6] Sepulveda-Jauregui et al. 2015, and [7] Repo et al. 2007.

Table 5. Isotopic fractionation $\delta^{13}\text{C}$ of CH_4 and CO_2 dissolved in surface and bottom waters at KWK and BGR sites (August 2015), and the separation factor ϵ_c in these lakes ($\delta^{13}\text{C}$ versus VPDB, mean \pm SD, $n = 3$).

Lake	$\delta^{13}\text{C}\text{-CH}_4$ (\pm SD) (‰)	$\delta^{13}\text{C}\text{-CO}_2$ (\pm SD) (‰)	ϵ_c (‰)
Surface			
KWK1	-45.7 (0.5)	-14.8 (0.3)	30.9
KWK11	-46.2 (0.0)	-16.2 (0.0)	30.0
KWK12	-47.0 (0.1)	-14.2 (0.3)	32.8
Average	-46.3 (0.2)	-15.1 (0.2)	31.2
Bottom			
KWK1	-66.1 (0.0)	-17.4 (0.0)	48.7
KWK11	-56.6 (0.8)	-18.1 (0.5)	38.4
KWK12	-67.0 (1.6)	-22.3 (1.7)	44.8
Average	-63.2 (0.8)	-19.3 (0.7)	44.0
Surface			
BGR1	-47.9 (0.5)	-13.8 (1.3)	34.1
BGR2	-48.2 (4.1)	-16.1 (2.7)	32.1
BGRb	-30.7 (0.3)	-15.8 (0.3)	14.9
Average	-42.3 (1.6)	-15.2 (1.4)	27.1
Bottom			
BGR1	-55.2 (3.7)	-13.6 (1.8)	41.6
BGR2	-47.1 (0.2)	-17.7 (1.0)	29.4
BGRb	-51.8 (0.7)	-12.1 (1.7)	39.7
Average	-51.4 (1.5)	-14.5 (1.5)	36.9

Note: VPDB, Vienna Pee Dee Belemnite.

Fig. 7. Isotopic fractionation $\delta^{13}\text{C}$ of CO_2 and CH_4 in surface and bottom waters of the lakes sampled at KWK and BGR sites, and the separation factor ϵ_c in these lakes (data from August 2015).

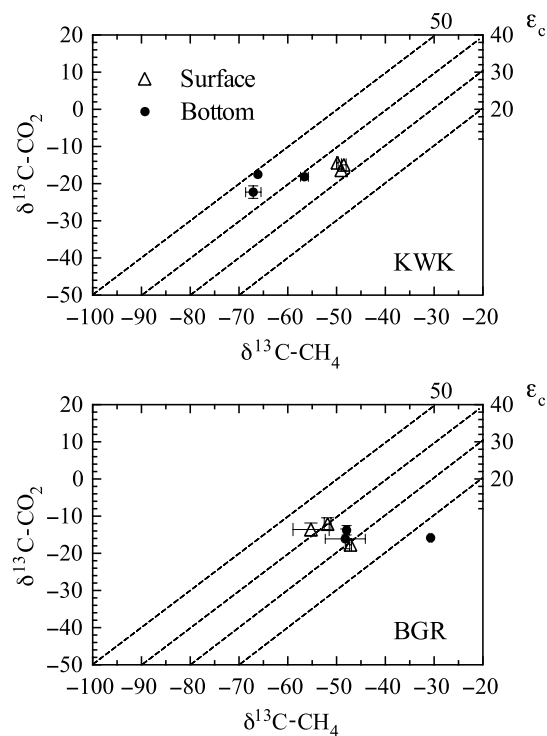
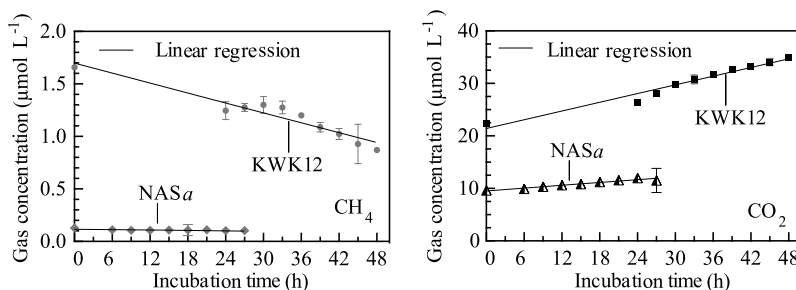


Fig. 8. The concurrent CH_4 oxidation and CO_2 accumulation rates in lake water sampled from NASa and KWK12, estimated as linear regressions of dissolved gas concentrations (data from August 2014) measured every 3 h in the water incubated for 27–48 h.



KWK ($0.38 \pm 0.02 \mu\text{mol CH}_4 \text{ L}^{-1} \text{ day}^{-1}$, $R^2 = 0.92$) compared with NAS ($0.016 \pm 0.002 \mu\text{mol CH}_4 \text{ L}^{-1} \text{ day}^{-1}$, $R^2 = 0.94$). These values corresponded to 5.7% (KWK) and 0.8% (NAS) of the measured net CO_2 production rates.

Discussion

Landscape changes in the region of the present study were most evident in the BGR area, with deepening, expansion and fusion of lakes, and the creation of new lakes (Fig. 2). These effects of the northward contraction and rapid degradation of permafrost have been well documented at BGR (Calmels et al. 2008). Changes of similar origin and scale were observed in the past at the southern end of our sampling region, the KWK valley site, during the period 1930–1960 (Allard and Seguin 1987). Over more recent decades, however, the total areal extent of lithalsa lakes in degraded permafrost region has remained relatively constant (Bouchard et al. 2014). Despite the older age, the KWK lakes continued to retain water up to a depth of almost 3 m, with strong stratification and anoxic bottom layers indicating intense microbial activity.

The diffusion rates of both CO_2 and CH_4 were much greater in the KWK lakes than at the more northerly sites where permafrost was less degraded, particularly relative to the NAS lakes. The rates of high diffusion exceeded those for ebullition at all measured sites. This contrasts with many reports for thermokarst lakes elsewhere, where ebullition was the dominant flux (Casper et al. 2000; Bastviken et al. 2011; Wik et al. 2013; Sepulveda-Jauregui et al. 2015). It remains possible that our limited sampling of ebullition missed important periods and places of intense ebullition, and that the values presented here are underestimates. The largest ebullition fluxes that have been observed elsewhere are persistent point sources (“seeps” and “hotspots”, as in Anthony et al. 2010), which are identifiable in the lake ice-cover (Wik et al. 2011; Lindgren et al. 2016). However, our continuous automated camera imaging of the lake surfaces did not reveal any persistent point ebullition in these lakes, nor were such hotspots observed during the sampling campaigns in four consecutive years. Thus, the undersampling error in our estimates of the ebullition flux seems unlikely to be large. It is possible, however, that our estimates of diffusion flux may have included quasi-stable microbubbles of gas (Prairie and del Giorgio 2013) that form in the supersaturated bottom waters and rise up through the water column (Matveev et al. 2016).

The total CH_4 efflux rates varied among sites and, to a lesser degree, among years and month of sampling, but at all locations the rates were substantial (Table 3). The maximum combined emission rate per unit area of $1.2 \text{ g CO}_2\text{-eq m}^{-2} \text{ day}^{-1}$ was observed in the KWK site experiencing accelerated permafrost degradation. However, the larger northernmost

lakes of the NAS site were emitting a similar amount of gas per lake, even although only diffusive fluxes were measured there (Table 3). The KWK lithalsa lakes, which lie in the most degraded permafrost region, had minimal ebullition rates ($7.2 \text{ mg CO}_2\text{-eq m}^{-2} \text{ day}^{-1}$ versus rates of $2450 \text{ mg CO}_2\text{-eq m}^{-2} \text{ day}^{-1}$ for lakes elsewhere reported in Wik et al. 2016), and were the smallest of all the studied lithalsa sites in terms of lake area (Supplementary Table S1¹). Despite these features, they still emitted an estimated $72.3 \text{ kg CO}_2\text{-eq year}^{-1}$, as high as the recently formed BGRb. The camera images also indicated that they had a two-week longer open-water period, which would favour a more prolonged period of emission.

Although these rates generally fall within the range of emissions reported elsewhere, they are less than those of palsa lakes in the same region (Table 4). Palsa lakes show similar pattern of emissions dominated by diffusion, but their organic-rich nature and intense bacterial activity (Deshpande et al. 2016) creates anoxic conditions through most of the water column (Deshpande et al. 2017), with abundant methanogenic communities (Crevecoeur et al. 2016) and thus high rates of methanogenesis. Even the oxygenated strata of these waters may be sites of methanogenesis, as recorded in oxic environments elsewhere (Bogard et al. 2014), and CH_4 production may be favoured by anoxic microenvironments within the organic particles that occur in high concentration in these waters.

The gas concentrations and emission rates measured here were made during the summer period of open water, and future studies will need to consider the full annual cycle. Continuous oxygen data from these subarctic waters indicate prolonged anoxia under the winter ice-cover, with mixing of the water column that may be delayed until convective overturn in autumn (Deshpande et al. 2015, 2017). Additional CH_4 and CO_2 sampling would therefore be of particular interest during the late winter ice-cover, spring ice-out, and fall cooling periods. Variations are also likely at much shorter timescales. The lithalsa lakes contain moderate Chl-*a* levels (Table 1), and phytoplankton as well as aquatic macrophytes may cause diurnal fluctuations in O_2 , CO_2 , and possibly also CH_4 . Previous studies with the CO_2 -box on the KWK lakes, for example, have provided initial indications of such diurnal cycles in all three gases (see Fig. 7c in Laurion et al. 2010). Nocturnal cooling and convective mixing may also influence emission rates (Anthony and MacIntyre 2016).

CH_4 oxidation

Our laboratory experiments indicate active methanotrophy taking place in these waters under oxygenated conditions, as was expected from previous 16S RNA analyses showing the presence of abundant methanotrophs in these waters (Crevecoeur et al. 2015). In both the KWK and NAS lakes this contributed a small fraction (around 1%–6%) of the total microbial respiration rate, consistent with the high rates of bacterial heterotrophy in thermokarst waters (Roiha et al. 2015; Deshpande et al. 2016). It is also consistent with the ^{14}C data that showed large differences in age between the two GHG because CO_2 derived from CH_4 oxidation would yield the same age (see below). The CH_4 oxidation rates (0.016 and $0.38 \mu\text{mol CH}_4 \text{ L}^{-1} \text{ day}^{-1}$, respectively, for NAS and KWK lakes) are at the low end of the range reported in other environments, for example 0.02 – $1.3 \mu\text{mol CH}_4 \text{ L}^{-1} \text{ day}^{-1}$ in the surface waters of a boreal lake in Finland (Kankaala et al. 2006). Much higher rates (1.2 – $33.8 \mu\text{mol CH}_4 \text{ L}^{-1} \text{ day}^{-1}$) were reported from Alaskan lakes across a range of landscapes in summer, however these estimates were derived from longer term (10–12 days) incubations after CH_4 enrichment (Martinez-Cruz et al. 2015). The CH_4 oxidation rates observed in the present study also imply that methanotrophy in lithalsa lakes is a much slower loss process than efflux to the atmosphere: the turnover time for CH_4 in KWK12 based on these measured oxidation rates would be 4.4 days, but only 2.8 days based on emission to the atmosphere from the upper 1 m of the water column; the equivalent turnover rates for NASa would be 8.1 (CH_4 oxidation) and 0.9 days (efflux). Rapid production and diffusion of

CH₄ from deeper waters and sediments to the surface waters of the lake would be needed to maintain the CH₄ concentrations above air-equilibrium, and seems unlikely to be a limiting factor for methanotrophy in these waters, where inorganic nutrient supply may impose a greater constraint.

Isotopic signatures

The analysis of isotopic signatures of CH₄ and CO₂ in lithalsa lakes showed large variability in their emission sources. The ¹⁴C dating of ebullition samples indicated that microbial community in at least one of these lakes has access to an ancient (mid-Holocene) carbon source, probably of the same postglacial origin as in the other lithalsa lakes in the region (Bouchard et al. 2014). The $\Delta^{14}\text{C}$ values of CO₂ emitted by ebullition from lake BGR1 varied by a factor of two, with a maximum age of around 6000 years. The $\Delta^{14}\text{C}$ values of CH₄ in the same samples from BGR1 also varied by about a factor of two, but corresponded to more modern ages (100–320 years B.P.). This divergence in $\Delta^{14}\text{C}$ signatures, with values corresponding to a much older age of the CO₂ carbon versus that of CH₄, implies at least partial separation of the pathways for production of the two gases. It is important to note however that the CO₂ ebullition flux measured at BGR is only about 4% of CH₄ ebullition flux (about 37% at KWK), so this old carbon source may have a negligible impact in terms of greenhouse effect. Differences in age have been found in other studies in the region and further north in the Canadian Arctic (Negandhi et al. 2013; Bouchard et al. 2015; Matveev et al. 2016), and sometimes with the reverse trend showing older CH₄ associated with methanogenesis based on old organic carbon released from degrading permafrost (Matveev et al. 2016). The older CO₂ measured here could potentially be derived from subsurface flows into the lake that pick up this gas from soil decomposition processes, including from thermokarst organic soils as described in the Alaskan tundra by Kling et al. (1991). Younger CH₄ could be derived from vegetation that occurs at the edge of and within the lithalsa lakes, and that is broken down by anaerobic processes in the bottom waters and sediments. However, the data are limited and will require corroboration with more extensive sampling and analyses.

The analysis of the $\delta^{13}\text{C}$ signatures showed a marked difference between the lithalsa lakes in discontinuous permafrost (BGR) versus those in the largely degraded permafrost (KWK). This difference was especially apparent in the bottom waters, which, in most of these lakes, would be little affected by aerobic oxidation of CH₄ that would deplete the $\delta^{13}\text{C}$ of the remaining CH₄. More depleted (i.e., more negative) values of $\delta^{13}\text{C}$ -CH₄ have been attributed to the differential use of lighter substrate carbon by methanogens (Whiticar 1999; Conrad 2005; Sancu and Panarello 2015). This also leads to carbon isotope separation between CH₄ and CO₂, which can indicate the methanogenic pathways that predominate (Whiticar 1999; Galand et al. 2010). In particular, Whiticar (1999) showed that carbon isotope separation factor ϵ_{C} [eq. (2)] in the range of 40‰–55‰ is most commonly associated with methylated substrate fermentation prevailing in freshwater environments, whereas higher and lower values were linked to acetoclastic (AM) and hydrogenotrophic (HM) pathways of CH₄ production, respectively, with some overlap on both sides (Galand et al. 2010; Penger et al. 2012; Vaughn et al. 2016). The ϵ_{C} values observed in the lithalsa lakes mostly fall at the edge between the ranges associated with HM and AM. This is in line with the analysis of archaeal 16S rRNA in these lakes (Crevecoeur et al. 2016), which found methanogens of the orders Methanomicrobiales (hydrogenotrophic) and Methanosarcinales (multiple pathways) to co-occur in abundance as the dominant Archaea. The lower ϵ_{C} values observed in the surface waters of the lithalsa lakes relative to those in the bottom waters (Table 3) could potentially be linked to CH₄ oxidation in the oxygenated epilimnion. The more depleted

$\delta^{13}\text{C-CH}_4$ values observed in the bottom of the KWK lakes (Table 5) may be linked to a greater degree of the substrate depletion by the methanogens.

Conclusions

Our subarctic observations indicate that lithalsa lakes begin emitting CH_4 and CO_2 as soon as they are formed. These emissions are through ebullition and diffusion pathways, and are liable to continue and accelerate, particularly via diffusive fluxes, as the permafrost continues to warm and erode. CH_4 oxidation appears to have a variable effect in reducing the stocks and therefore diffusive transfers of this gas to the atmosphere; at NAS the oxidation rates were a factor of 10 less than emission rates (11% of the calculated efflux from the upper metre of the water column to the atmosphere), but at KWK the oxidation rates were equivalent to around 63% of emissions, indicating a substantive reduction of potential emission rates by methanotrophy. Despite this effect of CH_4 oxidation, the KWK lakes were stronger emitters of CH_4 than at northern sites, and also emitted more CO_2 per unit area. Detailed surveys of lake sizes and density distributions will be needed to fully extrapolate these findings to the landscape scale. However, if the southern KWK lakes can be considered a space for time proxy for future change (Blois et al. 2013), these observations imply that thermokarst development in the lithalsa dominated landscape will be accompanied by increased GHG emissions, and that the lakes will persist as strong sources for at least many decades.

Acknowledgements

We acknowledge the support of the Centre d'études nordiques (CEN), the Natural Sciences and Engineering Research Council of Canada (NSERC) including the Discovery Frontiers project ADAPT, the Canada Research Chair program, the Canada First Research Excellence Funds program Sentinel North (BOND), the Quebec Nature and Technology Research funds (FRQNT), and the Northern Science Training Program. We also thank Valentin Prout for permission to reproduce the bathymetric data in Supplementary Fig. S3,¹ Tursujuq National Park (Kativik Regional Government) for permission to sample at BGR and NAS, two anonymous reviews for their valuable comments and suggestions, and all of those who helped us in the field and laboratory.

References

- Allan, J., Ronholm, J., Myktyczuk, N.C.S., Greer, C.W., Onstott, T.C., and Whyte, L.G. 2014. Methanogen community composition and rates of methane consumption in Canadian High Arctic permafrost soils. *Environ. Microbiol. Rep.* **6**: 136–144. doi: [10.1111/1758-2229.12139](https://doi.org/10.1111/1758-2229.12139). PMID: [24596286](https://pubmed.ncbi.nlm.nih.gov/24596286/).
- Allard, M., and Seguin, M.-K. 1987. Le pergélisol au Québec nordique : bilan et perspectives. *Géogr. Phys. Quat.* **41**: 141–152. doi: [10.7202/032671ar](https://doi.org/10.7202/032671ar). PMID: [29683143](https://pubmed.ncbi.nlm.nih.gov/29683143/).
- American Public Health Association (APHA), American Water Works Association (AWWA), and Water Environment Federation (WEF). 1998. Standard methods for the examination of water and wastewater. 20th ed. United Book Press, Inc., Baltimore, Md., USA.
- Anthony, K.M.W., and MacIntyre, S. 2016. Biogeochemistry: nocturnal escape route for marsh gas. *Nature*, **535**: 363–365. doi: [10.1038/535363a](https://doi.org/10.1038/535363a). PMID: [27443738](https://pubmed.ncbi.nlm.nih.gov/27443738/).
- Anthony, K.M.W., Vas, D.A., Brosius, L., Chapin, F.S., III, Zimov, S.A., and Zhuang, Q. 2010. Estimating methane emissions from northern lakes using ice-bubble surveys. *Limnol. Oceanogr. Methods*, **8**: 592–609. doi: [10.4319/lom.2010.8.0592](https://doi.org/10.4319/lom.2010.8.0592).
- Bastviken, D., Tranvik, L., Downing, J.A., Crill, P.M., and Enrich-Prast, A. 2011. Freshwater methane emissions offset the continental carbon sink. *Science*, **331**: 50. doi: [10.1126/science.1196808](https://doi.org/10.1126/science.1196808). PMID: [21212349](https://pubmed.ncbi.nlm.nih.gov/21212349/).
- Bégin, P.N., and Vincent, W.F. 2017. Permafrost thaw lakes and ponds as habitats for abundant rotifer populations. *Arct. Sci.* **3**: 354–377. doi: [10.1139/as-2016-0017](https://doi.org/10.1139/as-2016-0017).
- Bhiry, N., Delwaide, A., Allard, M., Bégin, Y., Fillion, L., Lavoie, M., Nozais, C., Payette, S., Pienitz, R., Saulnier-Talbot, É., and Vincent, W.F. 2011. Environmental change in the Great Whale River region, Hudson Bay: five decades of multidisciplinary research by Centre d'études nordiques (CEN). *Écoscience*, **18**: 182–203. doi: [10.2980/18-3-3469](https://doi.org/10.2980/18-3-3469).

- Blois, J.L., Williams, J.W., Fitzpatrick, M.C., Jackson, S.T., and Ferrier, S. 2013. Space can substitute for time in predicting climate-change effects on biodiversity. *Proc. Natl. Acad. Sci. USA*, **110**: 9374–9379. doi: [10.1073/pnas.1220228110](https://doi.org/10.1073/pnas.1220228110). PMID: 23690569.
- Bogard, M.J., del Giorgio, P.A., Boutet, L., Chaves, M.C.G., Prairie, Y.T., Merante, A., and Derry, A.M. 2014. Oxic water column methanogenesis as a major component of aquatic CH₄ fluxes. *Nat. Commun.* **5**: 5350. doi: [10.1038/ncomms6350](https://doi.org/10.1038/ncomms6350). PMID: 25355035.
- Bonilla, S., Villeneuve, V., and Vincent, W.F. 2005. Benthic and planktonic algal communities in a High Arctic lake: pigment structure and contrasting responses to nutrient enrichment. *J. Phycol.* **41**: 1120–1130. doi: [10.1111/j.1529-8817.2005.00154.x](https://doi.org/10.1111/j.1529-8817.2005.00154.x).
- Bouchard, F., Francus, P., Pienitz, R., Laurion, I., and Feyte, S. 2014. Subarctic thermokarst ponds: investigating recent landscape evolution and sediment dynamics in thawed permafrost of northern Québec (Canada). *Arct. Antarct. Alp. Res.* **46**: 251–271. doi: [10.1657/1938-4246-46.1.251](https://doi.org/10.1657/1938-4246-46.1.251).
- Bouchard, F., Laurion, I., Prieskienis, V., Fortier, D., Xu, X., and Whitticar, M.J. 2015. Modern to millennium-old greenhouse gases emitted from ponds and lakes of the Eastern Canadian Arctic (Bylot Island, Nunavut). *Biogeosciences*, **12**: 7279–7298. doi: [10.5194/bg-12-7279-2015](https://doi.org/10.5194/bg-12-7279-2015).
- Bouchard, F., MacDonald, L.A., Turner, K.W., Thienpont, J.R., Medeiros, A.S., Biskaborn, B.K., Korosi, J., Hall, R.L., Pienitz, R., and Wolfe, B.B. 2017. Paleolimnology of thermokarst lakes: a window into permafrost landscape evolution. *Arct. Sci.* **3**: 91–117. doi: [10.1139/as-2016-0022](https://doi.org/10.1139/as-2016-0022).
- Breton, J., Vallières, C., and Laurion, I. 2009. Limnological properties of permafrost thaw ponds in northeastern Canada. *Can. J. Fish. Aquat. Sci.* **66**: 1635–1648. doi: [10.1139/F09-108](https://doi.org/10.1139/F09-108).
- Calmels, F., Allard, M., and Delisle, G. 2008. Development and decay of a lithalsa in northern Québec: a geomorphological history. *Geomorphology*, **97**: 287–299. doi: [10.1016/j.geomorph.2007.08.013](https://doi.org/10.1016/j.geomorph.2007.08.013).
- Carignan, R. 1998. Automated determination of carbon dioxide, oxygen, and nitrogen partial pressures in surface waters. *Limnol. Oceanogr.* **43**: 969–975. doi: [10.4319/lo.1998.43.5.0969](https://doi.org/10.4319/lo.1998.43.5.0969).
- Casper, P., Maberly, S.C., Hall, G.H., and Finlay, B.J. 2000. Fluxes of methane and carbon dioxide from a small productive lake to the atmosphere. *Biogeochemistry*, **49**: 1–19. doi: [10.1023/A:1006269900174](https://doi.org/10.1023/A:1006269900174).
- Conrad, R. 2005. Quantification of methanogenic pathways using stable carbon isotopic signatures: a review and a proposal. *Org. Geochem.* **36**: 739–752. doi: [10.1016/j.orggeochem.2004.09.006](https://doi.org/10.1016/j.orggeochem.2004.09.006).
- Coplen, T.B. 2011. Guidelines and recommended terms for expression of stable-isotope-ratio and gas-ratio measurement results. *Rapid Commun. Mass Spectrom.* **25**: 2538–2560. doi: [10.1002/rcm.5129](https://doi.org/10.1002/rcm.5129). PMID: 21910288.
- Crevecoeur, S., Vincent, W.F., Comte, J., and Lovejoy, C. 2015. Bacterial community structure across environmental gradients in permafrost thaw ponds: methanotroph-rich ecosystems. *Front. Microbiol.* **6**: 192. doi: [10.3389/fmicb.2015.00192](https://doi.org/10.3389/fmicb.2015.00192). PMID: 25926816.
- Crevecoeur, S., Vincent, W.F., and Lovejoy, C. 2016. Environmental selection of planktonic methanogens in permafrost thaw ponds. *Sci. Rep.* **6**: 31312. doi: [10.1038/srep31312](https://doi.org/10.1038/srep31312). PMID: 27501855.
- Deshpande, B.N., MacIntyre, S., Matveev, A., and Vincent, W.F. 2015. Oxygen dynamics in permafrost thaw lakes: anaerobic bioreactors in the Canadian subarctic. *Limnol. Oceanogr.* **60**: 1656–1670. doi: [10.1002/lno.10126](https://doi.org/10.1002/lno.10126).
- Deshpande, B.N., Crevecoeur, S., Matveev, A., and Vincent, W.F. 2016. Bacterial production in subarctic peatland lakes enriched by thawing permafrost. *Biogeosciences*, **13**: 4411–4427. doi: [10.5194/bg-13-4411-2016](https://doi.org/10.5194/bg-13-4411-2016).
- Deshpande, B.N., Maps, F., Matveev, A., and Vincent, W.F. 2017. Oxygen depletion in subarctic peatland thaw lakes. *Arct. Sci.* **3**: 406–428. doi: [10.1139/as-2016-0048](https://doi.org/10.1139/as-2016-0048).
- Elvert, M., Pohlman, J.W., Becker, K.W., Gaglioti, B., Hinrichs, K.-U., and Wooller, M.J. 2016. Methane turnover and environmental change from Holocene lipid biomarker records in a thermokarst lake in Arctic Alaska. *Holocene*, **26**: 1766–1777. doi: [10.1177/0959683616645942](https://doi.org/10.1177/0959683616645942).
- Emmerton, C.A., St. Louis, V.L., Lehnherr, L., Graydon, J.A., Kirk, J.L., and Rondeau, K.J. 2016. The importance of freshwater systems to the net atmospheric exchange of carbon dioxide and methane with a rapidly changing high Arctic watershed. *Biogeosciences*, **13**: 5849–5863. doi: [10.5194/bg-13-5849-2016](https://doi.org/10.5194/bg-13-5849-2016).
- Galand, P.E., Yrjälä, K., and Conrad, R. 2010. Stable carbon isotope fractionation during methanogenesis in three boreal peatland ecosystems. *Biogeosciences*, **7**: 3893–3900. doi: [10.5194/bg-7-3893-2010](https://doi.org/10.5194/bg-7-3893-2010).
- Grosse, G., Jones, B., and Arp, C. 2013. 8.21. Thermokarst lakes, drainage, and drained basins. *In* Treatise on geomorphology. Edited by J.F. Shroder, R. Giardino, and J. Harbor. Academic Press, San Diego, Calif., USA. pp. 325–353. doi: [10.1016/B978-0-12-374739-6.00216-5](https://doi.org/10.1016/B978-0-12-374739-6.00216-5).
- Grosse, G., Goetz, S., McGuire, A.D., Romanovsky, V.E., and Schuur, E.A.G. 2016. Changing permafrost in a warming world and feedbacks to the Earth system. *Environ. Res. Lett.* **11**: 040201. doi: [10.1088/1748-9326/11/4/040201](https://doi.org/10.1088/1748-9326/11/4/040201).
- He, R., Wooller, M.J., Pohlman, J.W., Quensen, J., Tiedje, J.M., and Leigh, M.B. 2012. Shifts in identity and activity of methanotrophs in Arctic lake sediments in response to temperature changes. *Appl. Environ. Microbiol.* **78**: 4715–4723. doi: [10.1128/AEM.00853-12](https://doi.org/10.1128/AEM.00853-12). PMID: 22522690.
- Holgerson, M.A., and Raymond, P.A. 2016. Large contribution to inland water CO₂ and CH₄ emissions from very small ponds. *Nat. Geosci.* **9**: 222–226. doi: [10.1038/ngeo2654](https://doi.org/10.1038/ngeo2654).
- Huttunen, J.T., Alm, J., Liikanen, A., Juutinen, S., Larmola, T., Hammar, T., Silvola, J., and Martikainen, P.J. 2003. Fluxes of methane, carbon dioxide and nitrous oxide in boreal lakes and potential anthropogenic effects on the aquatic greenhouse gas emissions. *Chemosphere*, **52**: 609–621. doi: [10.1016/S0045-6535\(03\)00243-1](https://doi.org/10.1016/S0045-6535(03)00243-1). PMID: 12738299.
- Kanevskiy, M., Jorgenson, T., Shur, Y., O'Donnell, J.A., Harden, J.W., Zhuang, Q., and Fortier, D. 2014. Cryostratigraphy and permafrost evolution in the lacustrine lowlands of west-central Alaska. *Permafrost. Periglac. Process.* **25**: 14–34. doi: [10.1002/ppp.1800](https://doi.org/10.1002/ppp.1800).

- Kankaala, P., Huotari, J., Peltomaa, E., Saloranta, T., and Ojala, A. 2006. Methanotrophic activity in relation to methane efflux and total heterotrophic bacterial production in a stratified, humic, boreal lake. *Limnol. Oceanogr.* **51**: 1195–1204. doi: [10.4319/lo.2006.51.2.1195](https://doi.org/10.4319/lo.2006.51.2.1195).
- Kling, G.W., Kipphut, G.W., and Miller, M.C. 1991. Arctic lakes and streams as gas conduits to the atmosphere: implications for tundra carbon budgets. *Science*, **251**: 298–301. doi: [10.1126/science.251.4991.298](https://doi.org/10.1126/science.251.4991.298). PMID: [17733287](https://pubmed.ncbi.nlm.nih.gov/17733287/).
- Kokelj, S.V., and Jorgenson, M.T. 2013. Advances in thermokarst research. *Permafrost. Periglac. Process.* **24**: 108–119. doi: [10.1002/ppp.1779](https://doi.org/10.1002/ppp.1779).
- Laurion, I., Vincent, W.F., MacIntyre, S., Retamal, L., Dupont, C., Francus, P., and Pienitz, R. 2010. Variability in greenhouse gas emissions from permafrost thaw ponds. *Limnol. Oceanogr.* **55**: 115–133. doi: [10.4319/lo.2010.55.1.0115](https://doi.org/10.4319/lo.2010.55.1.0115).
- Lindgren, P.R., Grosse, G., Anthony, K.M.W., and Meyer, F.J. 2016. Detection and spatiotemporal analysis of methane ebullition on thermokarst lake ice using high-resolution optical aerial imagery. *Biogeosciences*, **13**: 27–44. doi: [10.5194/bg-13-27-2016](https://doi.org/10.5194/bg-13-27-2016).
- Lipson, D.A., Raab, T.K., Parker, M., Kelley, S.T., Brislaw, C.J., and Jansson, J. 2015. Changes in microbial communities along redox gradients in polygonized Arctic wet tundra soils. *Environ. Microbiol. Rep.* **7**: 649–657. doi: [10.1111/1758-2229.12301](https://doi.org/10.1111/1758-2229.12301). PMID: [26034016](https://pubmed.ncbi.nlm.nih.gov/26034016/).
- Martinez-Cruz, K., Sepulveda-Jauregui, A., Anthony, K.M.W., and Thalasso, F. 2015. Geographic and seasonal variation of dissolved methane and aerobic methane oxidation in Alaskan lakes. *Biogeosciences*, **12**: 4595–4606. doi: [10.5194/bg-12-4595-2015](https://doi.org/10.5194/bg-12-4595-2015).
- Matveev, A., Laurion, I., Deshpande, B.N., Bhiry, N., and Vincent, W.F. 2016. High methane emissions from thermokarst lakes in subarctic peatlands. *Limnol. Oceanogr.* **61**(S1): S150–S164. doi: [10.1002/lno.10311](https://doi.org/10.1002/lno.10311).
- Myhre, G., Shindell, D., Bréon, F.-M., Collins, W., Fuglestad, J., Huang, J., Koch, D., Lamarque, J.-F., Lee, D., Mendoza, B., Nakajima, T., Robock, A., Stephens, G., Takemura, T., and Zhang, H. 2013. Anthropogenic and natural radiative forcing. In *Climate change 2013: the physical science basis. Contribution of Working Group I to the Fifth Assessment Report of the Intergovernmental Panel on Climate Change. Edited by T.F. Stocker, D. Qin, G.-K. Plattner, M. Tignor, S.K. Allen, J. Boschung, A. Nauels, Y. Xia, V. Bex, and P.M. Midgley.* Cambridge University Press, Cambridge, UK and New York, N.Y., USA.
- Negandhi, K., Laurion, I., Whiticar, M.J., Galand, P.E., Xu, X., and Lovejoy, C. 2013. Small thaw ponds: an unaccounted source of methane in the Canadian high Arctic. *PLoS ONE*, **8**: e78204. doi: [10.1371/journal.pone.0078204](https://doi.org/10.1371/journal.pone.0078204). PMID: [24236014](https://pubmed.ncbi.nlm.nih.gov/24236014/).
- Payette, S., Delwaide, A., Caccianiga, M., and Beauchemin, M. 2004. Accelerated thawing of subarctic peatland permafrost over the last 50 years. *Geophys. Res. Lett.* **31**: L18208. doi: [10.1029/2004GL020358](https://doi.org/10.1029/2004GL020358).
- Penger, J., Conrad, R., and Blaser, M. 2012. Stable carbon isotope fractionation by methylotrophic methanogenic archaea. *Appl. Environ. Microbiol.* **78**: 7596–7602. doi: [10.1128/AEM.01773-12](https://doi.org/10.1128/AEM.01773-12). PMID: [22904062](https://pubmed.ncbi.nlm.nih.gov/22904062/).
- Pienitz, R., Bouchard, F., Narancic, B., Vincent, W.F., and Sarrazin, D. 2017. Seasonal ice cover and catchment changes at northern thermokarst ponds in Nunavik: observations from automated time-lapse cameras, v. 1.1 (2014–2016). *Nordica* **D24**. doi: [10.5885/45418AD-AF6A8064C702444B](https://doi.org/10.5885/45418AD-AF6A8064C702444B).
- Prairie, Y.T., and del Giorgio, P.A. 2013. A new pathway of freshwater methane emissions and the putative importance of microbubbles. *Inland Waters*, **3**: 311–320. doi: [10.5268/IW-3.3.542](https://doi.org/10.5268/IW-3.3.542).
- Proult, V. 2014. L'origine périglaciaire et son influence sur les écosystèmes thermokarstiques au Nunavik : analyse des communautés d'algues silicieuses. M.Sc. thesis, Université Laval, Québec, Que., Canada. 225 pp.
- Repo, M.E., Huttunen, J.T., Naumov, A.V., Chichulin, A.V., Lapshina, E.D., Bleuten, W., and Martikainen, P.J. 2007. Release of CO₂ and CH₄ from small wetland lakes in western Siberia. *Tellus Ser. B: Chem. Phys. Meteorol.* **59**: 788–796. doi: [10.1111/j.1600-0889.2007.00301.x](https://doi.org/10.1111/j.1600-0889.2007.00301.x).
- Roiha, T., Laurion, I., and Rautio, M. 2015. Carbon dynamics in highly heterotrophic subarctic thaw ponds. *Biogeosciences*, **12**: 7223–7237. doi: [10.5194/bg-12-7223-2015](https://doi.org/10.5194/bg-12-7223-2015).
- Sanci, R., and Panarello, H. 2015. Carbon and hydrogen isotopes as tracers of methane dynamic in wetlands. *Int. J. Geosci.* **6**: 720–728. doi: [10.4236/ijg.2015.67058](https://doi.org/10.4236/ijg.2015.67058).
- Sepulveda-Jauregui, A., Anthony, K.M.W., Martinez-Cruz, K., Greene, S., and Thalasso, F. 2015. Methane and carbon dioxide emissions from 40 lakes along a north–south latitudinal transect in Alaska. *Biogeosciences*, **12**: 3197–3223. doi: [10.5194/bg-12-3197-2015](https://doi.org/10.5194/bg-12-3197-2015).
- Stuiver, M., and Polach, H.A. 1977. Discussion: reporting of ¹⁴C data. *Radiocarbon*, **19**: 355–363. doi: [10.1017/S0033822200003672](https://doi.org/10.1017/S0033822200003672).
- Tan, Z., and Zhuang, Q. 2015. Arctic lakes are continuous methane sources to the atmosphere under warming conditions. *Environ. Res. Lett.* **10**: 054016. doi: [10.1088/1748-9326/10/5/054016](https://doi.org/10.1088/1748-9326/10/5/054016).
- Vachon, D., Prairie, Y.T., and Cole, J.J. 2010. The relationship between near-surface turbulence and gas transfer velocity in freshwater systems and its implications for floating chamber measurements of gas exchange. *Limnol. Oceanogr.* **55**: 1723–1732. doi: [10.4319/lo.2010.55.4.1723](https://doi.org/10.4319/lo.2010.55.4.1723).
- Vallée, S., and Payette, S. 2007. Collapse of permafrost mounds along a subarctic river over the last 100 years (northern Québec). *Geomorphology*, **90**: 162–170. doi: [10.1016/j.geomorph.2007.01.019](https://doi.org/10.1016/j.geomorph.2007.01.019).
- van Huissteden, J., Berrittella, C., Parmentier, F.J.W., Mi, Y., Maximov, T.C., and Dolman, A.J. 2011. Methane emissions from permafrost thaw lakes limited by lake drainage. *Nat. Clim. Change*, **1**: 119–123. doi: [10.1038/nclimate1101](https://doi.org/10.1038/nclimate1101).
- Vaughn, L.J.S., Conrad, M.E., Bill, M., and Torn, M.S. 2016. Isotopic insights into methane production, oxidation, and emissions in Arctic polygon tundra. *Glob. Change Biol.* **22**: 3487–3502. doi: [10.1111/gcb.13281](https://doi.org/10.1111/gcb.13281). PMID: [26990225](https://pubmed.ncbi.nlm.nih.gov/26990225/).

- Vincent, W.F., Lemay, M., and Allard, M. 2017. Arctic permafrost landscapes in transition: towards an integrated Earth system approach. *Arct. Sci.* **3**: 39–64. doi: [10.1139/as-2016-0027](https://doi.org/10.1139/as-2016-0027).
- Vonk, J.E., Tank, S.E., Bowden, W.B., et al. 2015. Effects of permafrost thaw on Arctic aquatic ecosystems. *Biogeosciences*, **12**: 7129–7167. doi: [10.5194/bg-12-7129-2015](https://doi.org/10.5194/bg-12-7129-2015).
- Walter, K.M., Zimov, S.A., Chanton, J.P., Verbyla, D., and Chapin, F.S. 2006. Methane bubbling from Siberian thaw lakes as a positive feedback to climate warming. *Nature*, **443**: 71–75. doi: [10.1038/nature05040](https://doi.org/10.1038/nature05040). PMID: [16957728](https://pubmed.ncbi.nlm.nih.gov/16957728/).
- Watanabe, S., Laurion, I., Pienitz, R., Chokmani, K., and Vincent, W.F. 2011. Optical diversity of thaw ponds in discontinuous permafrost: a model system for water color analysis. *J. Geophys. Res.: Biogeosci.* **116**: G02003. doi: [10.1029/2010JG001380](https://doi.org/10.1029/2010JG001380).
- Whiticar, M.J. 1999. Carbon and hydrogen isotope systematics of bacterial formation and oxidation of methane. *Chem. Geol.* **161**: 291–314. doi: [10.1016/S0009-2541\(99\)00092-3](https://doi.org/10.1016/S0009-2541(99)00092-3).
- Wik, M., Crill, P.M., Bastviken, D., Danielsson, Å., and Norbäck, E. 2011. Bubbles trapped in arctic lake ice: potential implications for methane emissions. *J. Geophys. Res.: Biogeosci.* **116**: G03044. doi: [10.1029/2011JG001761](https://doi.org/10.1029/2011JG001761).
- Wik, M., Crill, P.M., Varner, R.K., and Bastviken, D. 2013. Multiyear measurements of ebullitive methane flux from three subarctic lakes. *J. Geophys. Res.: Biogeosci.* **118**: 1307–1321. doi: [10.1002/jgrg.20103](https://doi.org/10.1002/jgrg.20103).
- Wik, M., Varner, R.K., Anthony, K.M.W., MacIntyre, S., and Bastviken, D. 2016. Climate-sensitive northern lakes and ponds are critical components of methane release. *Nat. Geosci.* **9**: 99–105. doi: [10.1038/ngeo2578](https://doi.org/10.1038/ngeo2578).
- Zimov, S.A., Voropaev, Y.V., Semiletov, I.P., Davidov, S.P., Prosiannikov, S.F., Chapin, F.S., III, Chapin, M.C., Trumbore, S., and Tyler, S. 1997. North Siberian lakes: a methane source fueled by Pleistocene carbon. *Science*, **277**: 800–802. doi: [10.1126/science.277.5327.800](https://doi.org/10.1126/science.277.5327.800).